

Supporting Information for: *The Different Interactions of Lysine and*

Arginine Side Chains with Lipid Membranes.

Libo Li^{†¶}, Igor Vorobyov[†] and Toby W. Allen^{†¶*},

[†]Department of Chemistry, University of California, Davis, USA.

[‡]School of Applied Sciences and Health Innovations Research Institute,

RMIT University, Melbourne, Australia.

Solvation analysis

Mean first-shell solvation numbers (shown in main text Figs. 3 and 8B) were determined by calculating the number of atoms within the 1st minimum of the Lys and Arg side chain – membrane component radial distribution functions (RDFs). Solvation numbers for Lys systems were calculated relative to its analog or side chain N atom with the 1st shell defined by radii 3.50, 3.20, and 3.65 Å for water oxygen, phosphate oxygen, and carbonyl oxygen, respectively. For Arg systems solvation numbers were computed relative to the central carbon atom of guanidine/guanidinium, with 1st solvation shells defined by radii 4.85, 4.55, and 5.00 Å for water oxygen, phosphate oxygen, and carbonyl oxygen, as in our previous studies¹⁻². These solvation numbers are compared in Figs. 3, 8B, and S6. To provide a more direct comparison between Arg and Lys, solvation numbers for methyl-guanidinium, MguanH⁺, shown in Fig.S7A as dashed lines, were computed relative its 3 N atoms with 1st solvation shells defined by radii 3.23, 3.20, and 3.45 Å for water oxygen, phosphate oxygen, and carbonyl oxygen, respectively, and compared to solvation numbers for methyl-ammonium, MamH⁺ (solid lines) in the figure.

In Fig. S7B we show MguanH⁺ and MamH⁺ solvation numbers from panel A divided by a number of H-bond donors for each molecule, e.g. 5 and 3, respectively, to assess the relative solvation capacity of these analogs. For MguanH⁺ this number is ~1 throughout the membrane, indicating that practically all O atoms in the 1st solvation shell form H-bonds. For MamH⁺ this number is ~1.5, suggesting it can accommodate 50% more O atoms than its H-bond capacity due to strong Coulomb interactions with its localized charge.

All solvation number profiles for Arg and Lys analogs (Figs. 3, 8B and S7) were symmetrized and errors represent a measure of asymmetry i.e. $|N(z) - N(-z)|/2$. For the analogs we also computed solvation numbers for all coordinating oxygen atoms (pink lines in Figs. 3, 8B and S7), which represent the sum of solvation numbers for water, lipid phosphate and carbonyl O. These estimates do not include a contribution from glycerol ester O atoms, though this is a small contribution (e.g. for MguanH⁺ it is ~0.09 on average, and up to 0.25 ± 0.10 at $|z| = 14$ Å, and within the uncertainties). Charged Arg and Lys side chain and analogs are also solvated by Cl⁻ counterions in the outer interfacial region (e.g. up to ~0.5 for

MguanH⁺; within 3.93 Å of the N atoms), but Cl⁻ solvation drops to 0 inside the membrane and is not considered further in this study.

Uncertainty measures

In all main text figures error bars for Arg and Lys side chain analogs (core number, solvation number, H-bond number and interaction energy profiles) were obtained from asymmetries as $|X(z) - X(-z)|/2$, for profile $X(z)$. For potentials of mean force (PMF) and pK_a shift profiles (Figs. 10 and 12), which have been set to 0 at reference points in bulk solution ($|z'| = 30$ Å), asymmetries were obtained as $|\{X(z) - X(z')\} - \{X(-z) - X(-z')\}|/2$. Error bars for pK_a shifts (Fig.12) were computed using propagation of errors. In the case of Mam in DPPC, the average/maximum uncertainties were 0.19/0.32.

For Arg and Lys side chains on TM helices, TM helix directionality and preferred side chain conformations prevent the use of asymmetry as a measure of statistical uncertainty¹. For these PMFs we have used standard error of means from four blocks (each of ~2 ns for each umbrella sampling window), with arbitrarily bulk reference adjusted to minimize root mean square deviations for entire PMFs. For MguanH⁺ and Mguan⁰ systems, PMF errors were computed from block analysis previously,² with average/maximum uncertainties of 0.15/0.29 and 0.11/0.32 kcal/mol, respectively. We note that PMF errors from asymmetries (0.39/1.06 kcal/mol and 0.14/0.40 kcal/mol, respectively) are similar to those from block analysis for neutral Mguan⁰, but larger for charged MguanH⁺ system, indicating some net force acting across the membrane for the charged molecule.³

Work decomposition analysis

In order to understand the origins of Arg and Lys side chain analog free energy barriers in Fig. 10A, we have decomposed them to contributions from individual polar components (water molecules, lipid head groups and ions; Fig. S14). As done previously, contributions from salt ions and lipid head groups are combined, and that from lipid hydrocarbon tails are not shown.

In force decomposition of charged analogs (Fig. S14A), large opposing contributions from water and head group+ions can be seen. At the interface, interaction force from water leads to a barrier of ~ 50 kcal/mol for MamH⁺ (Fig. S14A, solid red), cancelled by opposing contributions from lipid head groups (solid blue). In the middle of the membrane, water molecules are actually stabilizing MamH⁺ by ~ 65 kcal/mol, while lipid head groups are destabilizing it by ~ 80 kcal/mol. The reason is that, when MamH⁺ approaches the interface, it forms favorable interactions with lipid head groups, and breaks existing interactions between water and head groups. Thus, head groups are attracting MamH⁺ to the interface while water molecules there are expelling it. However, when MamH⁺ enters the hydrocarbon core, it deforms the membrane and causes considerable strains, leading to repulsive contributions from lipid head groups. On the other hand, without the interference of lipid head groups, water molecules better solvate MamH⁺ and stabilize it.

The force decomposition of Mam⁰ (Fig. S14B, solid lines) shows a similar trend, but with much smaller magnitude, which is expected because its interactions are much weaker (cf. Fig. 6A and 6B). The other difference for Mam⁰ is the plateau of individual component

contributions in the hydrophobic core of the membrane, where Mam^0 is quite far from the interface and experience a uniform hydration environment.

The force decomposition of MguanH^+ (Fig. S14A, dashed lines) is quite similar to that for MamH^+ (though somewhat smaller in magnitude, especially in the interfacial region), while that of Mguan^0 (Fig. S14B, dashed lines) has substantially greater magnitude than Mam^0 's. This can be explained by that, MguanH^+ 's interaction energies are similar to MamH^+ 's, while Mguan^0 's are stronger than Mam^0 's (see Fig. 6B) due to substantially larger dipole moment for Mguan^0 (2.2 D vs. 1.6 D for Mam^0).

Electrostatic potential calculations

Electrostatic potentials, ϕ , were obtained by solution to Poisson's equation using trajectories from MD simulations saved every 0.2 ps (i.e. every 100th time step), as described previously.⁴ The PME POT plug-in⁵ of VMD⁶ was used to obtain 2D and 1D profiles using smearing factor $\kappa=0.34 \text{ \AA}^{-1}$. The translocating ion contribution was present in those electrostatic potential profiles (shown in Figs. 11 and S16-S18 below). The average potential at the position of the translocating ion, ϕ_{ion} , (Fig. S15) was calculated from MD trajectory frames as the negative of the average potential energy change due to the discharging of the ion.

Solvation free energies

Calculations of solvation and partitioning free energies into bulk solvents involved simulations where a solute was held (with a $0.5 \text{ kcal/mol/\AA}^2$ harmonic constraint) in the middle of pre-equilibrated TIP3P water and cyclohexane boxes composed of 200 and 128 solvent molecules, respectively, as done previously.⁷ Bulk solvation and partitioning free energies were determined from the difference in free energy between the solute in solvent and vacuum, or between two solvents, respectively, calculated using free energy perturbation (FEP)⁸ and the staged protocol developed by Deng and Roux.⁹ Simulations in bulk solvent were performed in the *NPT* ensemble at 298 K using 1 atm isotropic pressure coupling. Simulations of 600 ps, with the first 100 ps discarded, were performed for each value of the coupling and/or staging parameter, representing a total of 20 ns sampling for each calculation. Three independent runs were performed for each solute/solvent combinations using different initial velocity distributions and/or starting structures. Uncertainties were obtained as standard errors of means from different runs. All solvation and partitioning free energies were corrected for finite Lennard-Jones (LJ) cutoffs using average interaction energies between a solute and solvent¹⁰ and those for ionic species were also corrected for interfacial potential contributions¹¹, and PME net charge artifacts¹², using procedures previously described⁷. All hydration and partitioning free energies use the same reference state (1 mol/L) in all phases.

	MamH ⁺	MguanH ⁺	Mam ⁰	Mguan ⁰
$\Delta G_{\text{hyd,exp}}$	-71.9 ¹³	-62.02 ⁷	-4.569 ¹⁴	-11.2 ¹⁵
$\Delta G_{\text{hyd,calc}}$	-71.61 ± 0.04	-64.02 ± 0.07	-3.53 ± 0.02	-11.85 ± 0.15
$\Delta G_{\text{sol,calc}}(\text{cHex})$	-3.02 ± 0.08	-6.72 ± 0.07	-1.17 ± 0.05	-2.85 ± 0.21
$\Delta G_{\text{part,calc}}(\text{water} \rightarrow \text{cHex})$	68.83 ± 0.08	57.54 ± 0.10	2.36 ± 0.05	8.99 ± 0.26

Table S1. Solvation and partitioning free energies of Lys and Arg side chain analogs (in kcal/mol). $\Delta G_{\text{hyd,exp}}$ are experimental hydration free energies from references^{7, 13-15}. The value from reference¹³ (-76.4 kcal/mol) was adjusted by -4.5 kcal/mol to reflect the difference between the absolute hydration free energy of H⁺ used in that and our previous work.⁷ $\Delta G_{\text{hyd,calc}}$ are calculated hydration free energies using all-atom C27 force field. $\Delta G_{\text{sol,calc}}(\text{cHex})$ are C27 calculated solvation free energies in liquid cyclohexane. $\Delta G_{\text{part,calc}}(\text{water} \rightarrow \text{cHex})$ are C27 calculated bulk partitioning free energies between water and cyclohexane. Bulk hydration and partitioning free energies were obtained at 298 K and 1 atm pressure.

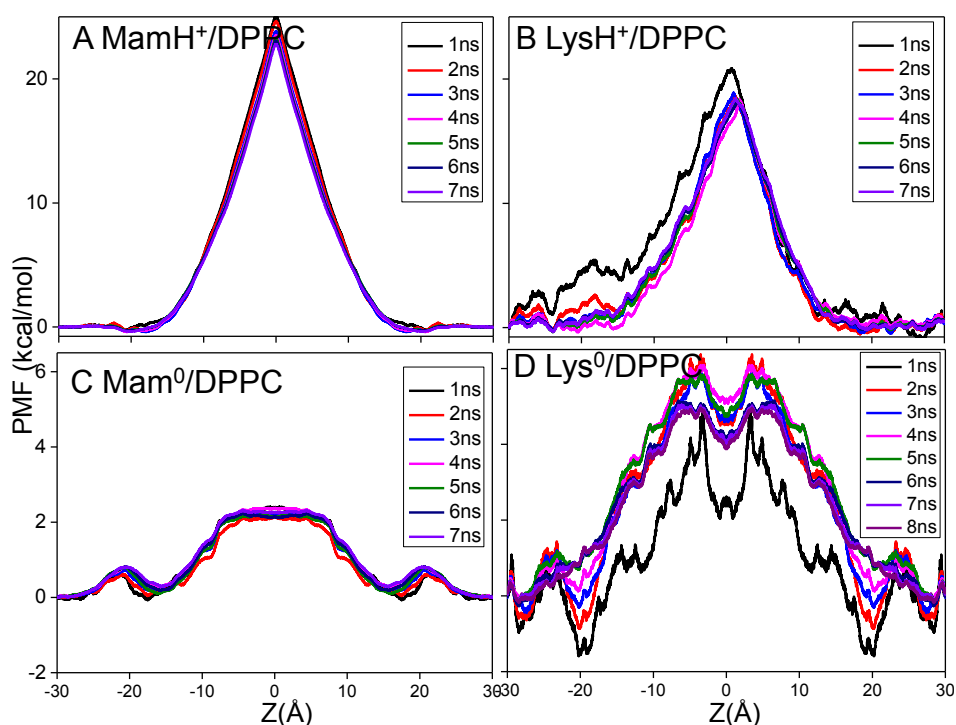


Figure S1. PMF convergence for 4 model systems: A, MamH⁺ (unsymmetrized); B, LysH⁺ (unsymmetrized); C, Mam⁰ (symmetrized); D, Lys⁰ (symmetrized), with convergence to within 0.5 kcal/mol.

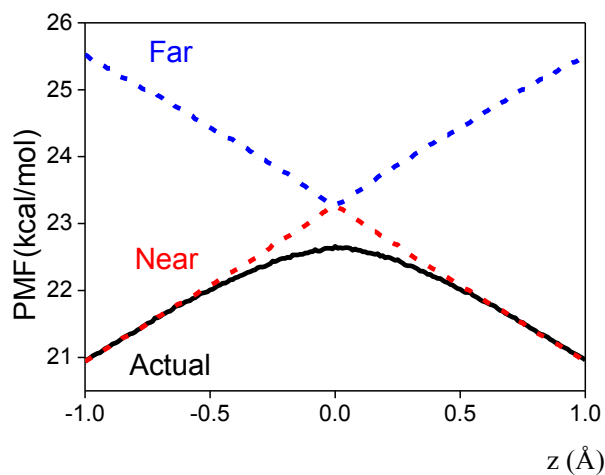


Figure S2. Far connection PMF (dashed blue), near connection PMF (dashed red) and actual PMF (solid black) for the MamH⁺/DPPC system.

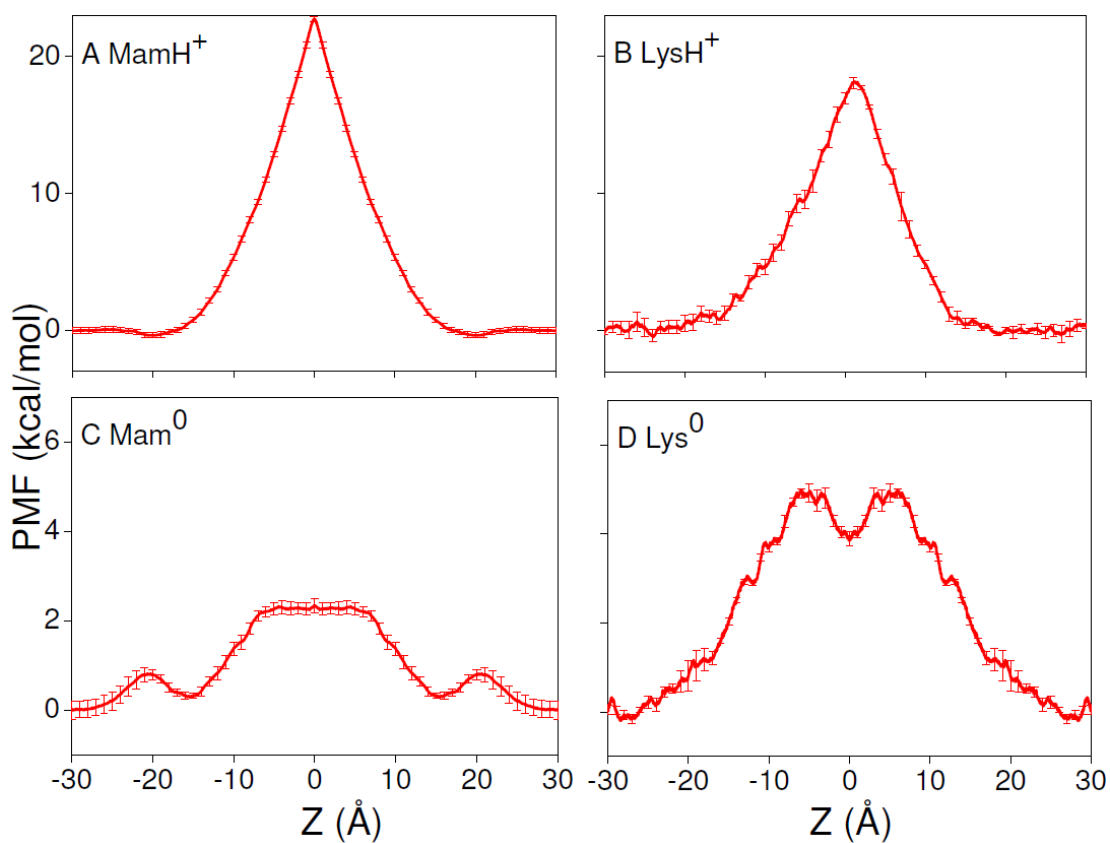


Figure S3. PMFs of 4 model DPPC systems with error bars (A: MamH⁺, B: LysH⁺, C: Mam⁰, D: Lys⁰), which are within 1 kcal/mol. Error bars are standard errors of mean from block analysis.

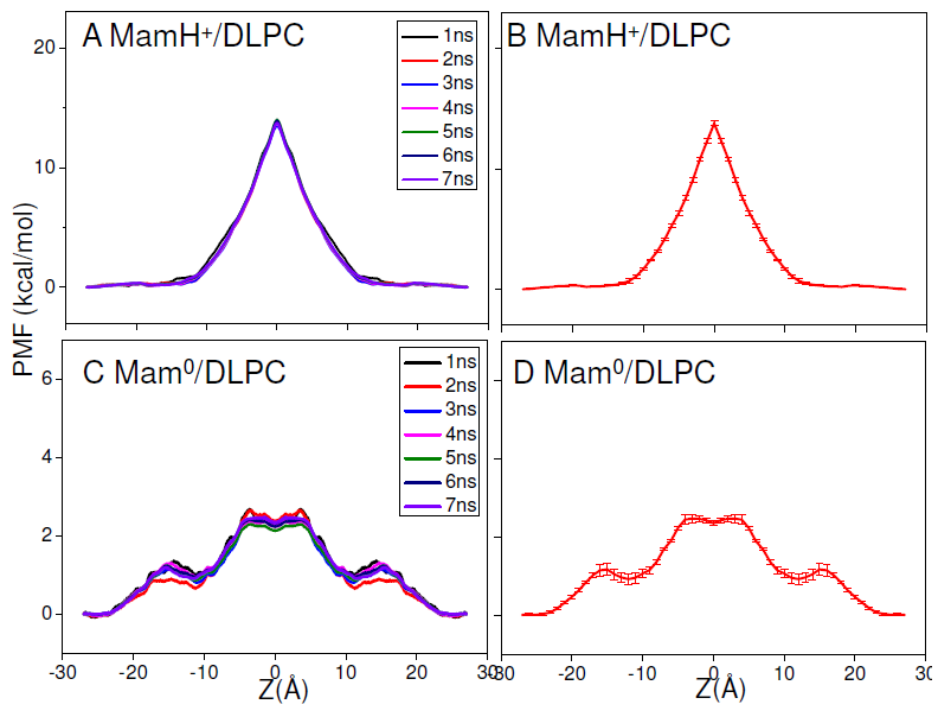


Figure S4. PMF convergence for 2 model DLPC systems, A: MamH⁺, C: Mam⁰; PMFs of 2 model DLPC systems with error bars, B: MamH⁺, D: Mam⁰. Error bars are standard errors of mean from block analysis.

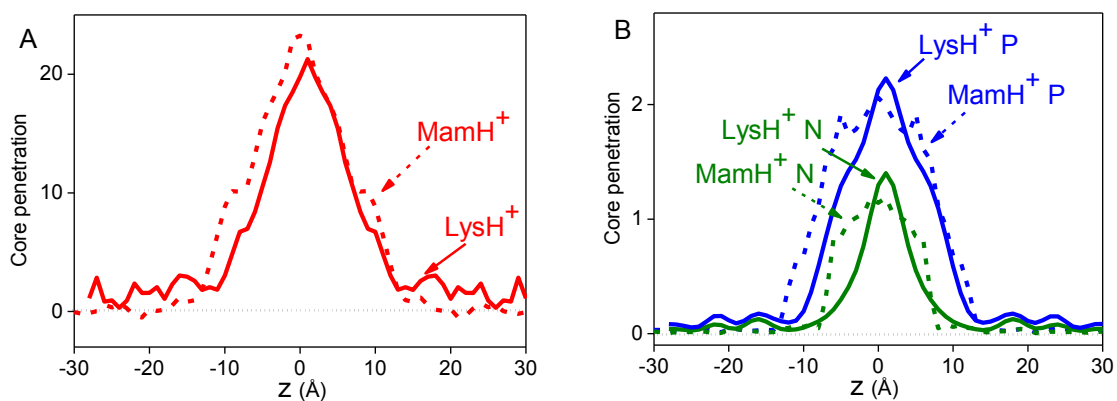


Figure S5. Penetration of molecules into the DPPC bilayer hydrocarbon core (defined as $|z| \leq 13 \text{ \AA}$) due to the insertion of MamH⁺ (dashed) or LysH⁺ (solid): for water (red), for lipid phosphate (blue) and choline groups (olive green) (A, B). The number of core-located water molecules is calculated with respect to those in an unperturbed bilayer.

Figure S6. Mean first-shell solvation numbers of LysH⁺(A), Lys⁰(B) for water oxygen (red), phosphate oxygen (blue), and lipid carbonyl oxygen (olive green) are shown as solid lines. Solvation numbers are the average number of atomic species within the first solvation shells defined by radii 3.50, 3.20, and 3.65 Å for water oxygen, phosphate oxygen, and carbonyl oxygen, respectively, relative to the central nitrogen atom of the side chain. The corresponding numbers for the Arg side chain, ArgH⁺(A), Arg⁰(B), are shown as dashed lines, with 1st solvation shells defined by radii 4.85, 4.55, and 5.00 Å for water oxygen, phosphate oxygen, and carbonyl oxygen, respectively, relative to the central carbon atom of guanidinium/guanidine.

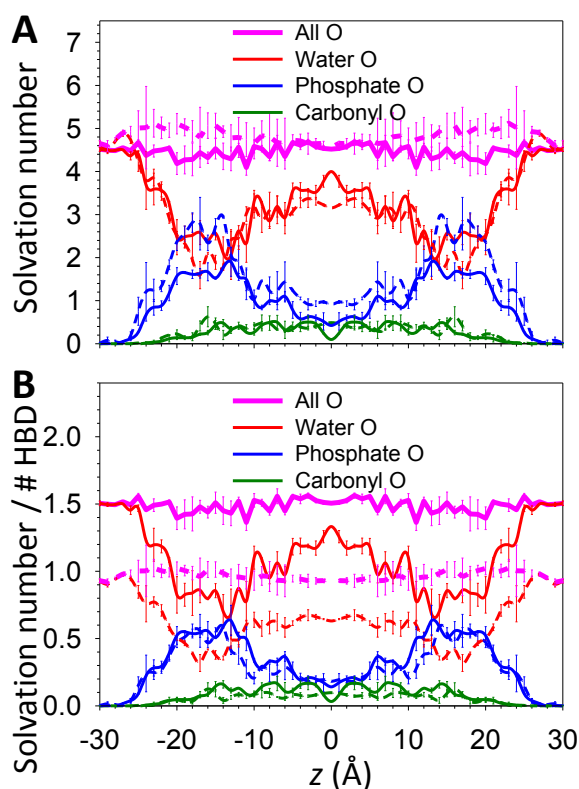
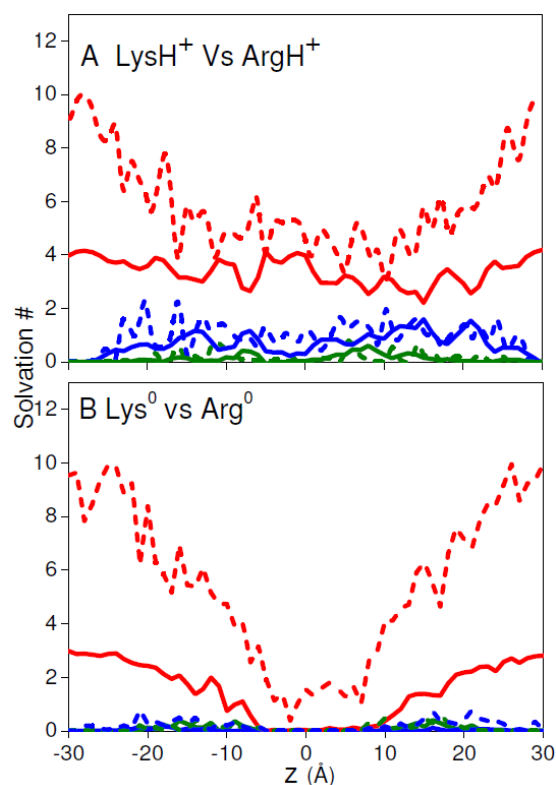


Figure S7. The average solvation numbers around the N atom of MamH⁺ (solid lines), compared to solvation numbers around all 3 N atoms of MguanH⁺ (dashed lines), calculated using MamH⁺/MguanH⁺ radii of: 3.50/3.23, 3.20/3.20, and 3.65/3.45 Å for water oxygen (red), phosphate oxygen (blue) and carbonyl oxygen (olive green) respectively. The total oxygen solvation number is shown as pink curves. Error bars represent asymmetry. Solvation numbers in panel (B) were divided by a number of hydrogen bond donors (HBD) per molecule (3 for MamH⁺ and 5 for MguanH⁺).

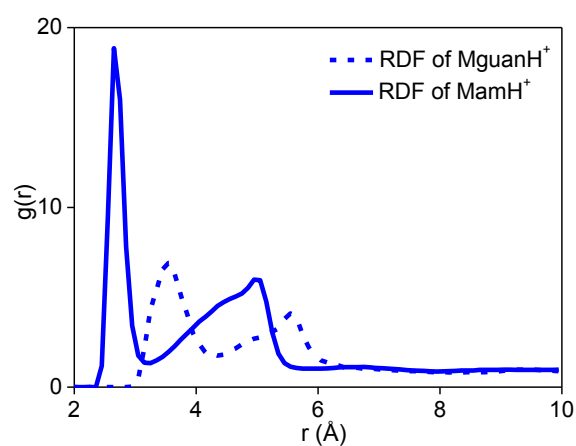


Figure S8. Typical radial distribution functions of phosphate oxygen atoms around MamH⁺ (its nitrogen atom) or MguanH⁺ (its central carbon atom) in DPPC.

Figure S9. The numbers of hydrogen bonds for LysH⁺ (A) and Lys⁰ (B) with water (red), lipid phosphate (blue) and carbonyl (olive). The total hydrogen bond numbers are shown as magenta. A hydrogen bond D-H \cdots A is defined when the distance H \cdots A < 2.5 \AA , and angle D-H \cdots A > 120 $^\circ$.

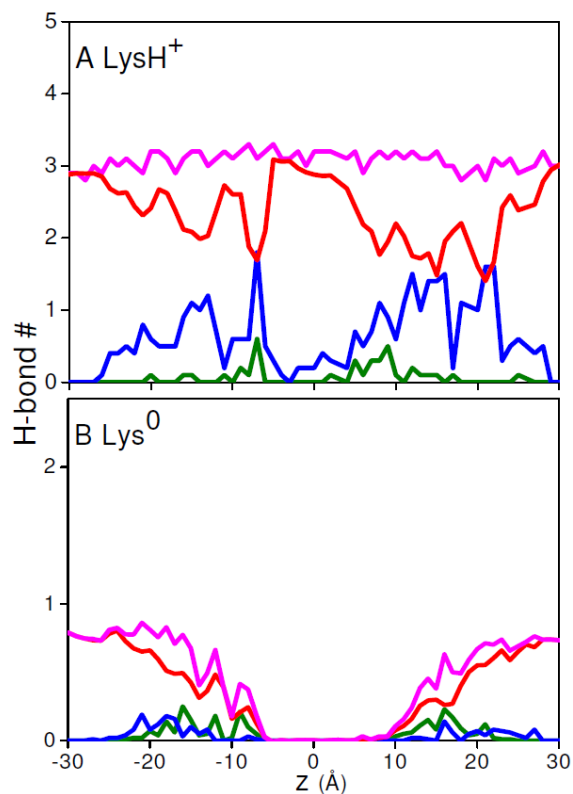


Figure S10. Average side chain interaction energies of LysH⁺ (A) and Lys⁰ (B) with components: water (red); lipid head groups, including carbonyl moieties (blue); K⁺ and Cl⁻ ions (cyan). The corresponding numbers of ArgH⁺ and Arg⁰ side chains are shown as dashed lines for comparison.

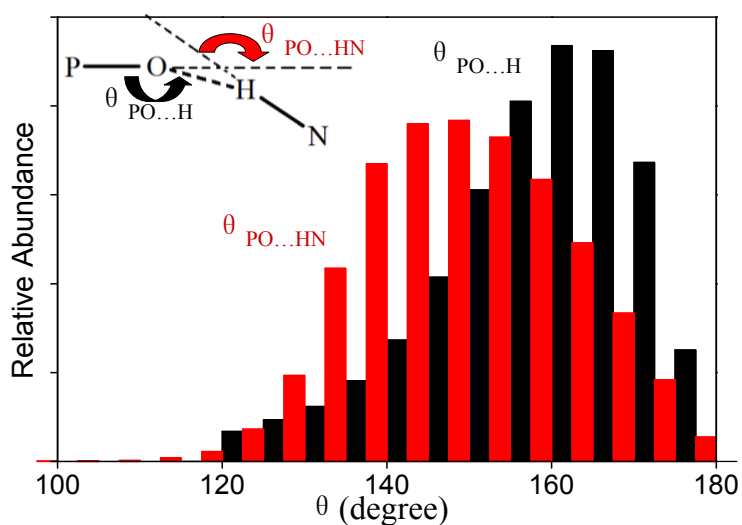
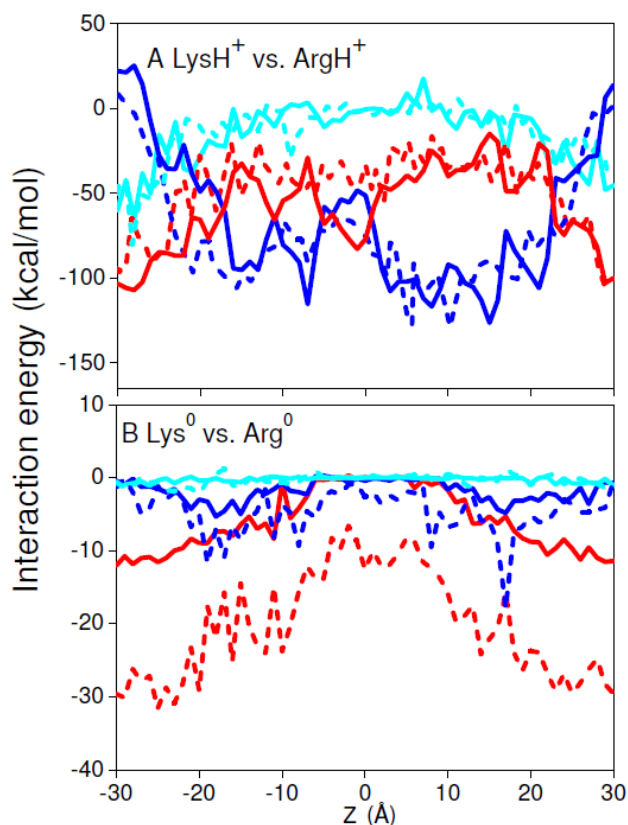


Figure S11. Distribution of angles PO...H and PO...HN (PO in the phosphate groups of lipids, and HN is in methyl-ammonium) for hydrogen bonding PO...HN in MamH⁺/DPPC simulations (counted over all simulation windows). These 2 angles are close to 180° (with maxima around 170° and 150°, respectively), representing a “co-linear” hydrogen bond.

Figure S12. (A) The distribution of different atoms (lipid phosphorus atom and water oxygen atoms) along the z -axis in DLPC simulations when $z = 0$. It is shown that MguanH^+ (dashed) pulls in head groups (red) and water (blue) molecules from both sides of the DLPC membrane while MamH^+ (solid) pulls in them only from one side. (B) Zoomed view of lipid P curves from panel A.

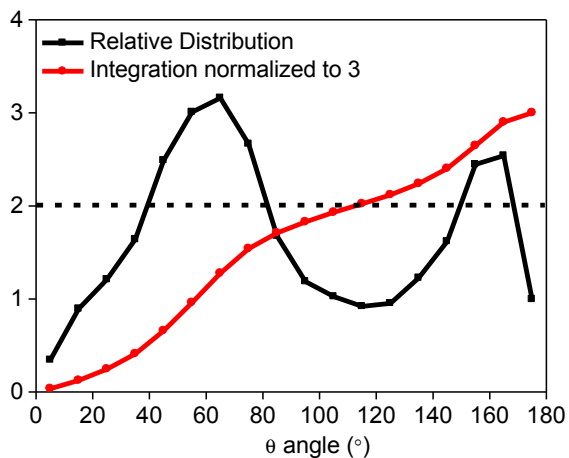
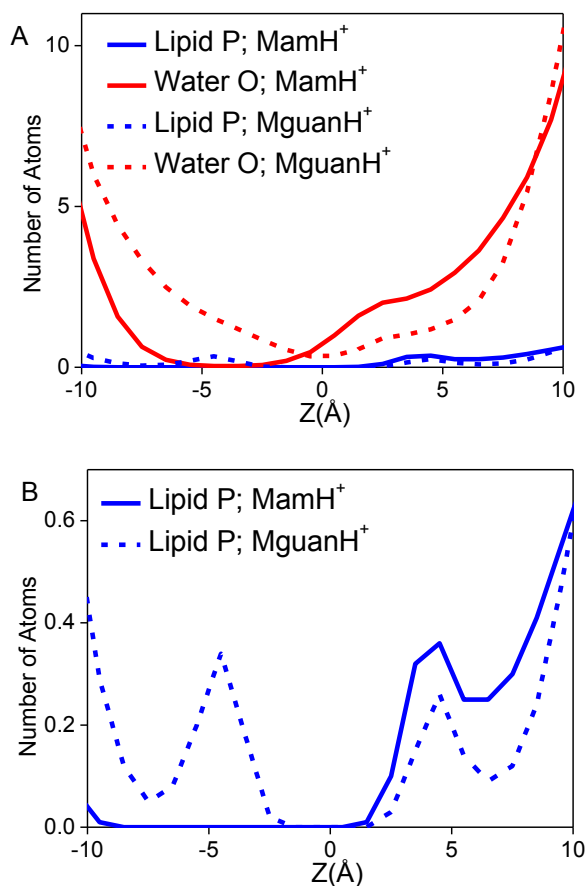


Figure S13. The relative distribution of angles (black) between C-N vectors of MguanH^+ and the z -axis (in DLPC membrane, see Fig. 9C in the main text), and its integration normalized to 3 (red). This indicates 1 C-N vector in MguanH^+ is parallel to the z -axis (the angle is close to 180°), while the other 2 form angles of about $\pm 60^\circ$ with the z -axis.

Figure S14. Free energy contributions from water (red), lipid head groups and K^+ , Cl^- ions (blue), obtained for $MamH^+$ (A), Mam^0 (B). Corresponding curves for $MguanH^+$ or $Mguan^0$ are shown as dashed lines.

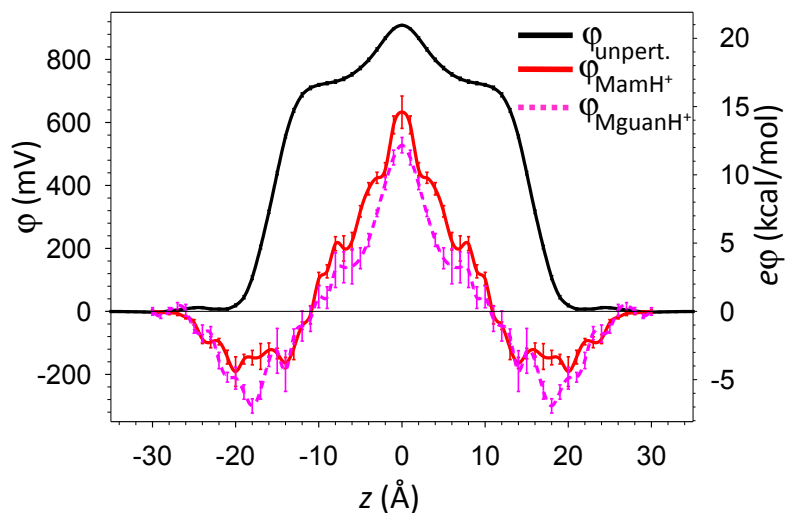
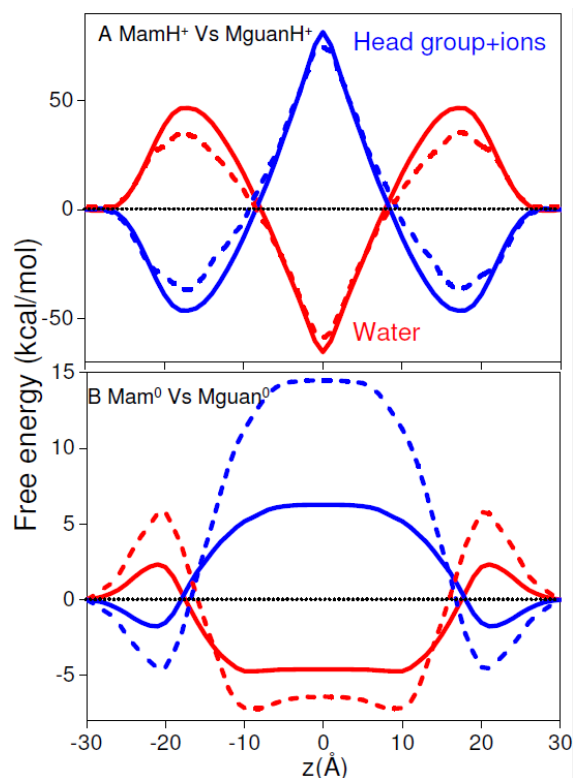


Figure S15. Electrostatic potential (ϕ) and energy ($e\phi$) difference associated with charging the translocating ion across the membrane. The electrostatic potential seen by a point +e charge across an unperturbed membrane (membrane dipole potential) is shown as black lines. Electrostatic potentials and energy contributions associated with $MamH^+$ and $MguanH^+$ translocation are shown as solid red and dashed pink lines, respectively. Note that results contain both short-range local solvation as well as long-range contributions. Error bars represent one standard error of means from block analysis.

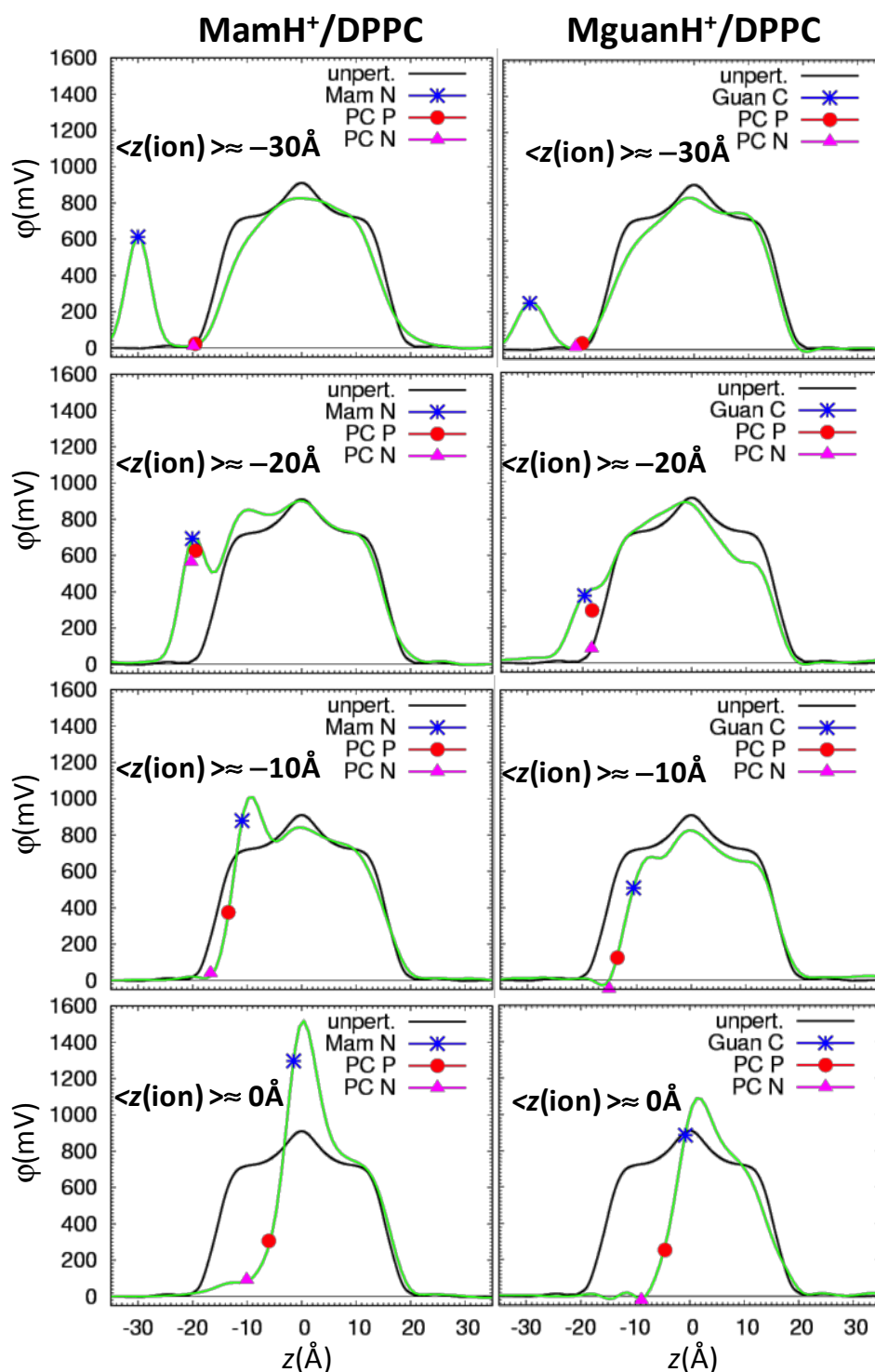


Figure S16. Electrostatics of the deformed DPPC membrane: 1D electrostatic potential profiles along the z axis for MamH⁺ (left panels) and MguanH⁺ (right panel) translocation for several positions, $\langle z(\text{ion}) \rangle$, across a DPPC bilayer from C27 simulations. Electrostatic potential profiles (green curves) were calculated for (x,y) passing through the average position of the ion (N atom for MamH⁺ or guanidine C for MguanH⁺) indicated by blue asterisks. Electrostatic potentials at the position of the closest to the ion lipid P and N atoms are shown by red circle and pink triangle. Profiles were calculated using PMEpot with $\kappa=0.34 \text{ \AA}^{-1}$ and referenced to bulk aqueous solution. Note that translocating molecular ion contribution to the potential is present in those profiles. See Figure 11 for corresponding 2D profiles. Electrostatic potential profiles for an unperturbed DPPC bilayer are shown as black curves.

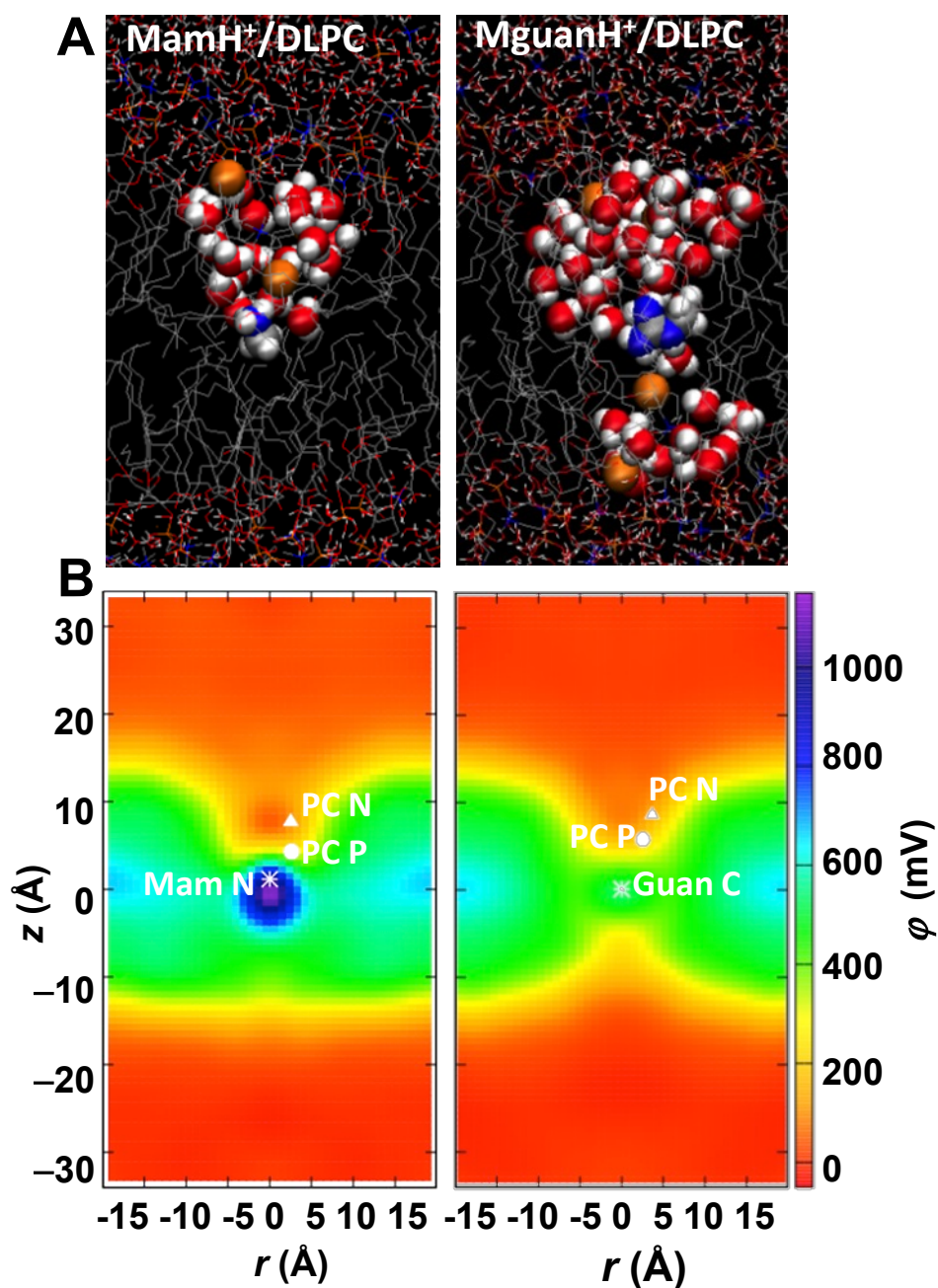


Figure S17. Electrostatics of the deformed DLPC membrane: **(A)** Equilibrated system snapshots and **(B)** 2D electrostatic potential maps along the z axis and distance r from the z axis when the MamH⁺ (left panels) or MguanH⁺ (right panels) ion is located near DLPC membrane center ($\langle z(\text{ion}) \rangle \approx 0 \text{ \AA}$). In panel **A** C atoms are gray, H are white, P are orange, O are red, and N are blue. The translocating molecular ion as well as lipid phosphate and water atoms that have been pulled into the bilayer core are drawn in space-filling representation. In panel **B**, the average positions of the ion (N for MamH⁺ and guanidine C for MguanH⁺) and its closest DLPC P and N atoms are shown as asterisk, circle and triangle, respectively. The corresponding 1D electrostatic potential profiles are shown in Fig.S18.

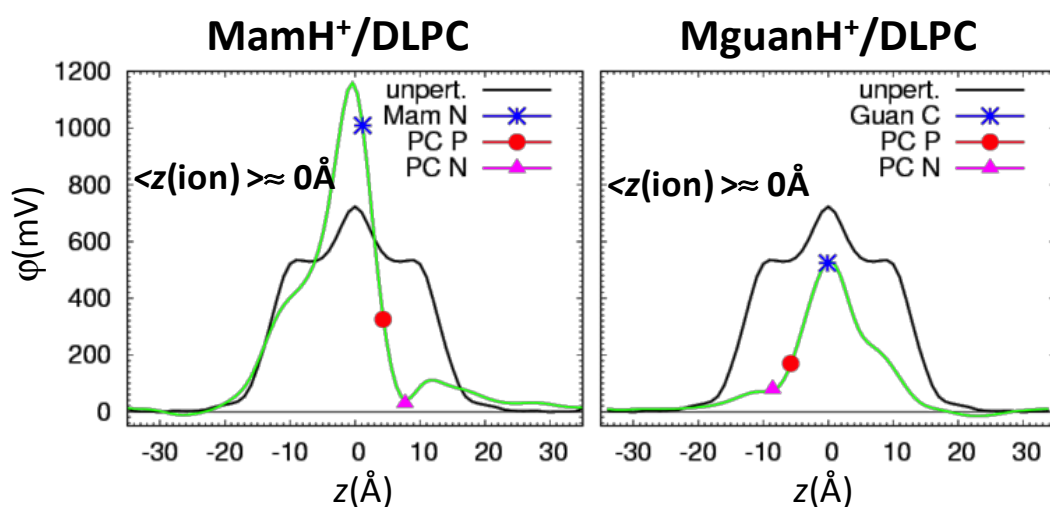
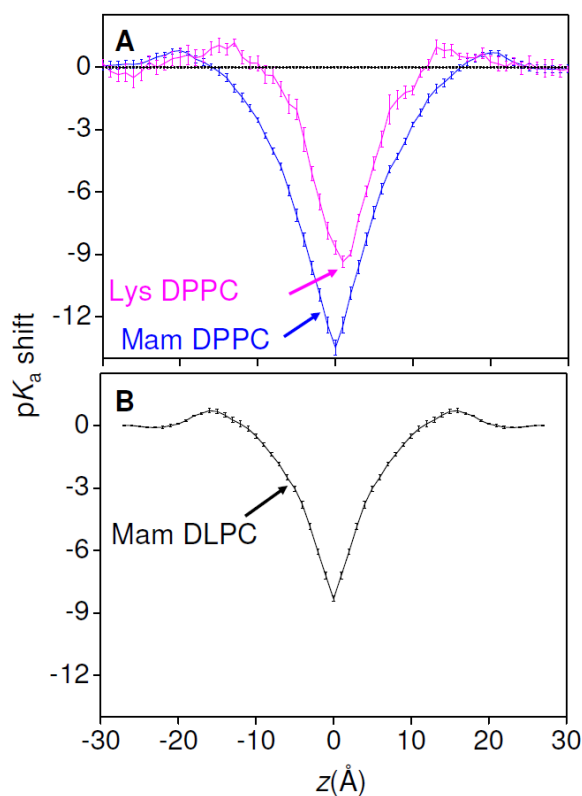


Figure S18. Electrostatics of the deformed DLPC membrane: 1D electrostatic potential profiles along the z axis for MamH⁺ (left panel) and MguanH⁺ (right pane) near DLPC membrane center ($\langle z(\text{ion}) \rangle \approx 0 \text{ \AA}$). Electrostatic potential profiles (green curves) were calculated for (x,y) passing through the average position of the ion (N atom for MamH⁺ or guanidine C for MguanH⁺) indicated by blue asterisks. Electrostatic potentials at the position of the closest to the ion lipid P and N atoms are shown by red circle and pink triangle. Profiles were calculated using PMEPT with $\kappa=0.34 \text{ \AA}^{-1}$ and referenced to bulk aqueous solution. Note that translocating molecular ion contribution to the potential is present in those profiles. See Figure S17 for corresponding 2D profiles. Electrostatic potential profiles for the unperturbed DLPC bilayer are shown as black curves.

Figure S19. (A) pK_a shift profiles for the Mam analog (solid blue) and Lys side chain (solid pink) in DPPC showing error bars. (B) pK_a shift profiles for Mam analog (solid black) in DLPC showing error bars. Refer to our previous publication¹⁶ for error bars for the Mguan system, which are similar.



Supporting References

1. Dorairaj, S.; Allen, T. W. On the thermodynamic stability of a charged arginine side chain in a transmembrane helix. *Proc. Natl. Acad. Sci. U. S. A.* **2007**, *104*, 4943-4948.
2. Li, L. B.; Vorobyov, I.; Allen, T. W. Potential of mean force and pK(a) profile calculation for a lipid membrane-exposed arginine side chain. *J. Phys. Chem. B* **2008**, *112*, 9574-9587.
3. Neale, C.; Bennett, W. F. D.; Tieleman, D. P.; Pomes, R. Statistical convergence of equilibrium properties in simulations of molecular solutes embedded in lipid bilayers. *J. Chem. Theory Comput.* **2011**, *7*, 4175-4188.
4. Vorobyov, I.; Bekker, B.; Allen, T. W. Electrostatics of deformable lipid membranes. *Biophys. J.* **2010**, *98*, 2904-2913.
5. Aksimentiev, A.; Schulten, K. Imaging alpha-hemolysin with molecular dynamics: Ionic conductance, osmotic permeability, and the electrostatic potential map. *Biophys. J.* **2005**, *88*, 3745-3761.
6. Humphrey, W.; Dalke, A.; Schulten, K. VMD: Visual molecular dynamics. *J. Mol. Graphics* **1996**, *14*, 33-38.
7. Vorobyov, I.; Li, L. B.; Allen, T. W. Assessing atomistic and coarse-grained force fields for protein-lipid interactions: The formidable challenge of an ionizable side chain in a membrane. *J. Phys. Chem. B* **2008**, *112*, 9588-9602.
8. Kollman, P. Free-Energy Calculations - Applications to Chemical and Biochemical Phenomena. *Chem. Rev.* **1993**, *93*, 2395-2417.
9. Deng, Y. Q.; Roux, B. Hydration of amino acid side chains: Nonpolar and electrostatic contributions calculated from staged molecular dynamics free energy simulations with explicit water molecules. *J. Phys. Chem. B* **2004**, *108*, 16567-16576.
10. Anisimov, V. M.; Vorobyov, I. V.; Roux, B.; MacKerell, A. D. Polarizable empirical force field for the primary and secondary alcohol series based on the classical drude model. *J. Chem. Theory Comput.* **2007**, *3*, 1927-1946.
11. Lamoureux, G.; Roux, B. Absolute hydration free energy scale for alkali and halide ions established from simulations with a polarizable force field. *J. Phys. Chem. B* **2006**, *110*, 3308-3322.
12. Bogusz, S.; Cheatham, T. E.; Brooks, B. R. Removal of pressure and free energy artifacts in charged periodic systems via net charge corrections to the Ewald potential. *J. Chem. Phys.* **1998**, *108*, 7070-7084.
13. Kelly, C. P.; Cramer, C. J.; Truhlar, D. G. Aqueous solvation free energies of ions and ion-water clusters based on an accurate value for the absolute aqueous solvation free energy of the proton. *J. Phys. Chem. B* **2006**, *110*, 16066-16081.
14. Ben-Naim, A.; Marcus, Y. Solvation thermodynamics of nonionic solutes. *J. Chem. Phys.* **1984**, *81*, 2016-2027.
15. Wolfenden, R.; Andersson, L.; Cullis, P. M.; Southgate, C. C. B. Affinities of amino acid side chains for solvent water. *Biochemistry* **1981**, *20*, 849-855.
16. Li, L. B. B.; Vorobyov, I.; Allen, T. W. The role of membrane thickness in charged protein-lipid interactions. *Biochim. Biophys. Acta, Biomembr.* **2012**, *1818*, 135-145.